Pseudoresonant interaction between flame and upstream velocity fluctuations

V. Karlin*
University of Central Lancashire, Preston PR1 2HE, United Kingdom
(Received 22 February 2005; published 24 January 2006)

This work is dedicated to the analysis of the delicate details of the effect of upstream velocity fluctuations on the flame propagation speed. The investigation was carried out using the Sivashinsky model of cellularization of hydrodynamically unstable flame fronts. We identified the perturbations of the steadily propagating flames which can be significantly amplified over finite periods of time. These perturbations were used to model the effect of upstream velocity fluctuations on the flame front dynamics and to study a possibility to control the flame propagation speed.

DOI: 10.1103/PhysRevE.73.016305 PACS number(s): 47.20.−k, 47.27.−i, 47.54.−r, 68.05.−n

I. INTRODUCTION

Experiments show that cellularization of flames results in an increase of their propagation speed. In order to understand and exploit this phenomenon, we study the evolution of flame fronts governed by the Sivashinsky equation

$$\partial_t \Phi - \frac{1}{2}(\partial_x \Phi)^2 = \partial_{xx}\Phi - \frac{\gamma}{2}\partial_x \mathcal{H}[\Phi] + f(x,t) \qquad (1)$$

for $-\infty < x < \infty$, $t > 0$. Here $\Phi(x,t)$ is the perturbation of the plane flame front, $f(x,t)$ is the the force term, $\mathcal{H}[\Phi] = \pi^{-1}\int_{-\infty}^{\infty}(x-\xi)^{-1}\Phi(\xi,t)d\xi$ is the Hilbert transformation, and $\gamma = 1 - \rho_b/\rho_u$ is the contrast in densities of burnt and unburnt gases ρ_b and ρ_u, respectively. Initial perturbation $\Phi(x,0)$ is given.

Equation (1) governs evolution of the perturbation $\Phi(x,t)$ of the plane flame front moving with the planar flame speed u_b relative to the burnt gases. Thus, at a given instant of time t, the surface of the flame front is described as the distance $t + \Phi(x,t)$ from a reference plane. For the unity Lewis number, space coordinates are expressed in units of the flame front width $\delta_{th} = D_{th}/u_b$ and time is in units of $\gamma^{-2}\delta_{th}/u_b$, where D_{th} is the thermal diffusivity of the system.

The equation without the force term was obtained in [1] as an asymptotic mathematical model of cellularization of flames subject to the hydrodynamic flame instability. The force term was suggested in [2] in order to account for the effect of the upstream turbulence on the flame front. It is equal to the properly scaled turbulent fluctuations of the velocity field of the unburned gas. In [3,4], Eq. (1) was further refined in order to include effects of the second order in γ. However, as mentioned in [4], this modification can be compensated upon a Galilean transformation combined with a nonsingular scaling. Thus, we have chosen to remain within the first order of accuracy in γ of the original Sivashinsky model (1) as it should have the same qualitative properties as the more quantitatively accurate one.

The asymptotically stable solutions to the Sivashinsky equation with $f(x,t) \equiv 0$ corresponding to the steadily propagating cellular flames do exist and are given by formula

$$\Phi_{N,L}(x,t) = V_{N,L}t + 2\sum_{n=1}^{N} \ln|\cosh 2\pi b_n/L - \cos 2\pi x/L|, \qquad (2)$$

discovered in [5]. Here, real $L > 0$ and integer N from within the range $0 \leq N \leq N_L = \mathrm{ceil}(\gamma L/8\pi + 1/2) - 1$ are otherwise arbitrary parameters. Also, $V_{N,L} = 2\pi N L^{-1}(\gamma - 4\pi N L^{-1})$, $b_1, b_2, \ldots, b_N$ satisfy a system of nonlinear algebraic equations available elsewhere, and ceil(x) is the smallest integer not less than x. Functions (2) have a distinctive set of N complex conjugate pairs of poles $z_n = \pm i b_n$, $n = 1, \ldots, N$, and are called the steady coalescent pole solutions, respectively.

The steady coalescent pole solutions (2) with the maximum possible number $N = N_L$ of poles were found to be asymptotically, for $t \to \infty$, stable if the wavelength of the perturbations does not exceed L; see [6]. However, in spite of their asymptotic stability, there are perturbations of these solutions which can be hugely amplified over finite intervals of time, resulting in significant transients; see [7]. These perturbations are nonmodal, because they cannot be represented by the single eigenmodes of the linearized Sivashinsky equation.

Note that L is an independent parameter in Eq. (2). Earlier numerical experiments (see, e.g., [8]) revealed that there is no particular period L inherent to Eq. (1). Generally speaking, numerical solutions to Eq. (1) in large, but finite computational domains, stabilize to Eq. (2) with the period L coinciding with the size of the computational domain. This makes it reasonable to study the periodic solutions to Eq. (1) with the period L considered as an independent parameter. Thus, in what follows we are interested in solutions (2) with $N = N_L$ and retain the index L only. Also, in all reported calculations $\gamma = 0.8$. Here, the computational domain is considered to be large if it is much greater than the wavelength $8\pi/\gamma$ of the harmonic, which is the most amplified one in the Darrieus-Landau instability.

In Sec. II we calculate the most amplifiable nonmodal perturbations to the asymptotically stable cellular solutions of the Sivashinsky equation. In Sec. III we reinforce numeri-

*Electronic address: VKarlin@uclan.ac.uk

cal investigations of Sec. II with the analytical analysis of a local approximation to the linearized Sivashinsky equation, which was suggested in [9]. Also, this analysis provides a test case to validate numerical studies of the response of the flame front to stochastic forcing or noise presented in Sec. IV. In particular, we investigate a possibility to model the stochastic forcing as a random sequence of the most amplifiable nonmodal perturbations of the Sivashinsky equation.

II. LARGEST GROWING PERTURBATIONS

A. Linear analysis

Substituting $\Phi(x,t)=\Phi_L(x,t)+\phi(x,t)$ into (1) for $f(x,t)\equiv 0$ and linearizing it with respect to the L-periodic perturbations $\phi(x,t)$, one obtains

$$\partial_t\phi = (\partial_x\Phi_L)\partial_x\phi + \partial_{xx}\phi - \frac{\gamma}{2}\partial_x\mathcal{H}[\phi] = A_L\phi,$$

$$\phi(x,0) = \Phi(x,0) - \Phi_L(x,0). \tag{3}$$

The operator A_L generates the evolution operator e^{tA_L}, which provides the solution to Eqs. (3) in the form $\phi(x,t)=e^{tA_L}\phi(x,0)$.

Assuming that the polar decomposition of the evolution operator does exist, we write it as

$$e^{tA_L} = \mathcal{U}(t)\mathcal{S}(t), \tag{4}$$

where $\mathcal{U}(t)$ is a partially isometric and $\mathcal{S}(t)=[(e^{tA_L})^* e^{tA_L}]^{1/2}$ is the nonnegative self-adjoint operator; see, e.g., [10]. The partial isometry of $\mathcal{U}(t)$ implies that it preserves the norm when mapping between the sets of values of $(e^{tA_L})^*$ and e^{tA_L}—i.e., $\|\mathcal{U}(t)\phi\|=\|\phi\|$. Then, under certain conditions, $\|\phi(x,t)\|=\|\mathcal{S}(t)\phi(x,0)\|$ and for the 2-norm the

$$\sup_{\phi(x,0)\in\mathcal{D}(e^{tA_L})}\{\|\mathcal{S}(t)\phi(x,0)\| \times \|\phi(x,0)\|^{-1}\}$$

is equal to the largest eigenvalue $\sigma_1(t)$ of $\mathcal{S}(t)$. This eigenvalue is associated with the eigenvector $\psi_1(x,t)$ of $\mathcal{S}(t)$. Here $(e^{tA_L})^*$ denotes the operator adjoint to e^{tA_L} and $\mathcal{D}(e^{tA_L})$ stands for the domain of definition of e^{tA_L}.

The eigenvectors $\psi_\alpha(x,t)$ of $\mathcal{S}(t)$ are mutually orthogonal at any given time $t=t^*$ and can be used as a basis in the space of the admissible initial conditions $\phi(x,0)=\sum_{\alpha=1}^{\infty}c_\alpha(0,t^*)\times\psi_\alpha(x,t^*)$. Then, the associated eigenvalues $\sigma_\alpha(t^*)$ provide the magnitudes of amplification of the $\psi_\alpha(x,t^*)$ components of the initial condition $\phi(x,0)$ by the time instance t^*. Note that for Eqs. (3) the 2-norm of the perturbation $\phi(x,t)$ is just its energy and that the eigenvalues $\sigma_\alpha(t)$, $\alpha=1,2,\ldots$, and eigenvectors $\psi_\alpha(x,t)$ of $\mathcal{S}(t)$ are the singular values and the right singular vectors of e^{tA_L}, respectively.

According to [11], the Fourier image $\widetilde{A_L}$ of the operator A_L is defined by the (k,l)th entry of its double-infinite $(-\infty<k,l<\infty)$ matrix

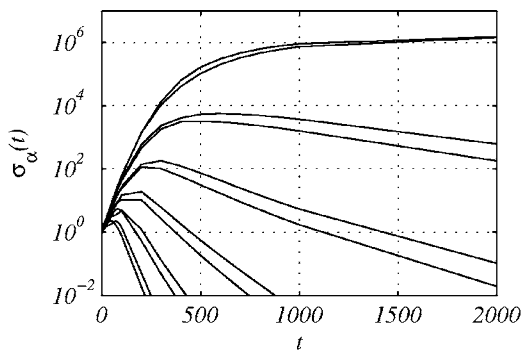

FIG. 1. Twelve largest singular values of e^{tA_L} for $L=40\pi$.

$$\widetilde{(A_L)}_{k,l} = \left(-\frac{4\pi^2}{L^2}k^2 + \frac{\pi\gamma}{L}|k|\right)\delta_{k,l} + \frac{8\pi^2}{L^2}l\,\mathrm{sgn}(k-l)\sum_{n=1}^{N_L} e^{-2\pi b_n|k-l|/L}, \tag{5}$$

where $\delta_{k,l}$ is the Kronecker's symbol. By limiting our consideration to the first K harmonics, we approximate our double-infinite matrix $\widetilde{A_L}$ with the $(2K+1)\times(2K+1)$ matrix $\widetilde{A_L}^{(K)}$, whose entries coincide with those of $\widetilde{A_L}$ for $-K\leqslant k, l\leqslant K$. Then, the matrix $e^{t\widetilde{A_L}^{(K)}}\approx e^{t\widetilde{A}_L}$ can be effectively evaluated by the scaling and squaring algorithm with a Padé approximation. Eventually, the required estimations of $\sigma_\alpha(t)$ and Fourier images of $\psi_\alpha(x,t)$ can be obtained through the singular-value decomposition (SVD) of $e^{t\widetilde{A_L}^{(K)}}$; see, e.g., [12].

Indeed, if the SVD of $e^{t\widetilde{A_L}^{(K)}}$ is given by

$$\widetilde{e^{tA_L^{(K)}}} = \mathcal{W}(t)\mathcal{B}(t)\mathcal{V}(t)^*, \tag{6}$$

where $\mathcal{W}(t)$, $\mathcal{V}(t)$ are unitary and $\mathcal{B}(t)$ is the non-negative diagonal matrix, then the matrices

$$\mathcal{U}(t) = \mathcal{W}(t)\mathcal{V}(t)^*, \quad \mathcal{S}(t) = \mathcal{V}(t)\mathcal{B}(t)\mathcal{V}(t)^* \tag{7}$$

satisfy the adequate finite-dimensional projection of the polar decomposition (4) and the eigenvalues $\sigma_\alpha(t)$, $\alpha=1,2,\ldots$, and eigenvectors $\psi_\alpha(x,t)$ of $\mathcal{S}(t)$ are just the singular values and the Fourier syntheses of the right singular vectors of $e^{t\widetilde{A}_L^{(K)}}$, respectively.

Graphs showing dependence of a few largest singular values of e^{tA_L} versus time are shown in Fig. 1. One may see that values of $\sigma_\alpha(t)$, $\alpha=1,2$, for large enough t match the estimation of the largest possible amplification of the perturbations $\phi(x,t)$ obtained in [7] by a different method. An even more impressive observation is that the dimension of the subspace of the significantly amplifiable perturbations is very low. Perturbations of only two types can be amplified by about 10^6 times.

The initial conditions $\phi(x,0)$, which would be the most amplified once by $t^*=100$, 300, and 10^3—i.e., $\psi_\alpha(x,t^*)$—are depicted in Fig. 2. The dominating singular modes $\psi_\alpha(x,t)$ stabilize to some limiting functions for $t>300$. For example, their graphs for $t=500$ and $t=10^3$ are indistinguishable in Fig. 2. However, they vary in time significantly when

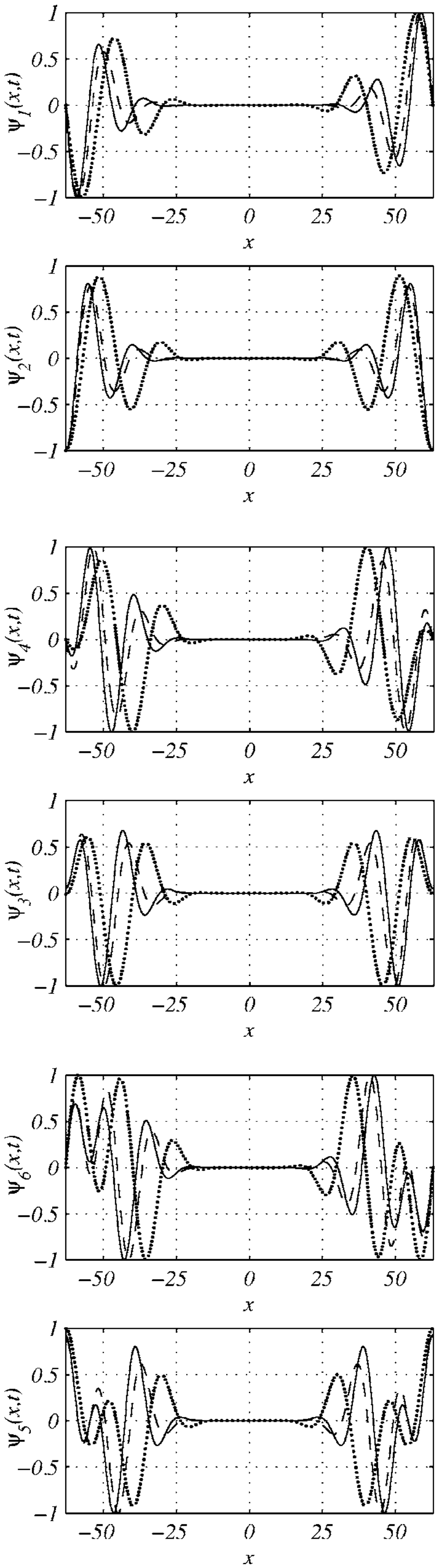

FIG. 2. Right singular vectors of e^{tA_L}, corresponding to the six largest $\sigma_\alpha(t)$ for $t=100$ (dotted line), 300 (dashed line), and 10^3 (solid line), are given in pairs of a symmetric and asymmetric one for $L=40\pi$. Here $\sigma_\alpha(10^3)\approx 9.2\times 10^5$ and 7.4×10^5 for $\alpha=1,2$, respectively. $\max\{\sigma_\alpha(t^*)\approx 5.7\times 10^3$ and 3.3×10^3 for $\alpha=3,4$, respectively, is reached for $t^*\approx 500$.

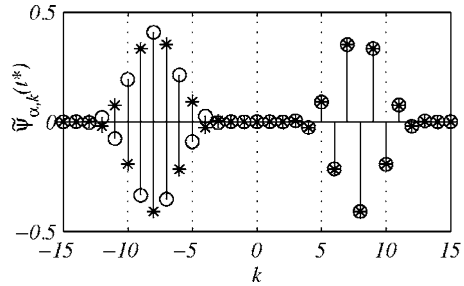

FIG. 3. Fourier coefficients of $\psi_\alpha(x,t^*)=\Sigma_{k=-\infty}^{\infty}\tilde{\psi}_{\alpha,k}(t^*)e^{i2\pi kx/L}$ for $t^*=10^3$; ○, $*$ correspond to $\alpha=1,2$, respectively; $L=40\pi$.

$t<300$ and for $t=200$ the associated amplification σ_α, $\alpha=1,2$, is already about 10^3, though $\psi_\alpha(x,200)$, $\alpha=1,2$, does not coincide with either $\psi_\alpha(x,10^3)$, $\alpha=1,2$, or $\psi_\alpha(x,10^3)$, $\alpha=3,4$. Thus, the dependence of ψ_α on time makes the dimension of the subspace of perturbations, which can be amplified to say about 10^3 times much higher than 2 in contrast to what could be concluded from the graphs in Fig 1. This illustrates the complicatedness of studies of the effect of transient amplification on short-time scales $t<300$.

Fourier components of $\psi_1(x,t^*)$ and $\psi_2(x,t^*)$ for $t^*=10^3$ are depicted in Fig. 3. Data for graphs in Figs. 1–3 were obtained for $K=256$, though similar to our analysis of the pseudospectra of $\tilde{A}_L^{(K)}$ in [11], first few singular values and singular vectors of $e^{t\tilde{A}_L^{(K)}}$ are well stabilized for $K\gtrsim 2L/\pi$.

One may see in Fig. 1 that $\sigma_\alpha(t)$, $\alpha=1,2$, do not decay as time grows, apparently contradicting the asymptotic stability of $\Phi_L(x,t)$. However, there is no contradiction at all, since solutions to the Sivashinsky equation are shift invariant and the asymptotic stability of $\Phi_L(x,t)$ is related to its shape rather than location. Indeed, if $\Phi(x,t)$ is a solution to Eq. (1) with $f(x,t)\equiv 0$, then $\Phi(x+C_1,t)+C_2$ is its solution too for any real C_1, C_2.

This shift invariance of Eq. (1) implies the existence of two zero eigenvalues of the operator A_L from Eqs. (3); see [6,11]. Thus, if $\phi(x,0)$ contains contributions from eigenvectors corresponding to the zero eigenvalues, then these contributions to $\phi(x,t)=e^{tA_L}\phi(x,0)$ will not vanish for $t\to\infty$. Instead, $e^{tA_L}\phi(x,0)$ will converge to $\Phi_L(x+C_1,t)+C_2-\Phi_L(x,t)$ with some real C_1, C_2. Note that because of the severe nonorthogonality of eigenvectors of A_L, even a substantial contribution of the zero eigenvector in $\phi(x,0)$ can be nearly canceled out by other eigenvectors, so that $\|\phi(x,0)\|\ll 1$. Similarly, $e^{tA_L}\psi_\alpha(x)$, $\alpha=1,2$, converge to $\Phi_L(x+C_1,t)+C_2-\Phi_L(x,t)$ with some different values of real C_1, C_2, and the corresponding $\sigma_\alpha(t)$ converge to the 2-norms of the above limits rather than to zero. Right singular vectors $\psi_\alpha(x)$ of orders higher than 2 do not include components of eigenvectors associated with the zero eigenvalues and corresponding singular values $\sigma_\alpha(t)$ vanish for $t\to\infty$.

B. Nonlinear numerical simulations

The evolution of the perturbations, which grow the most and are governed by the nonlinear Sivashinsky equation, is

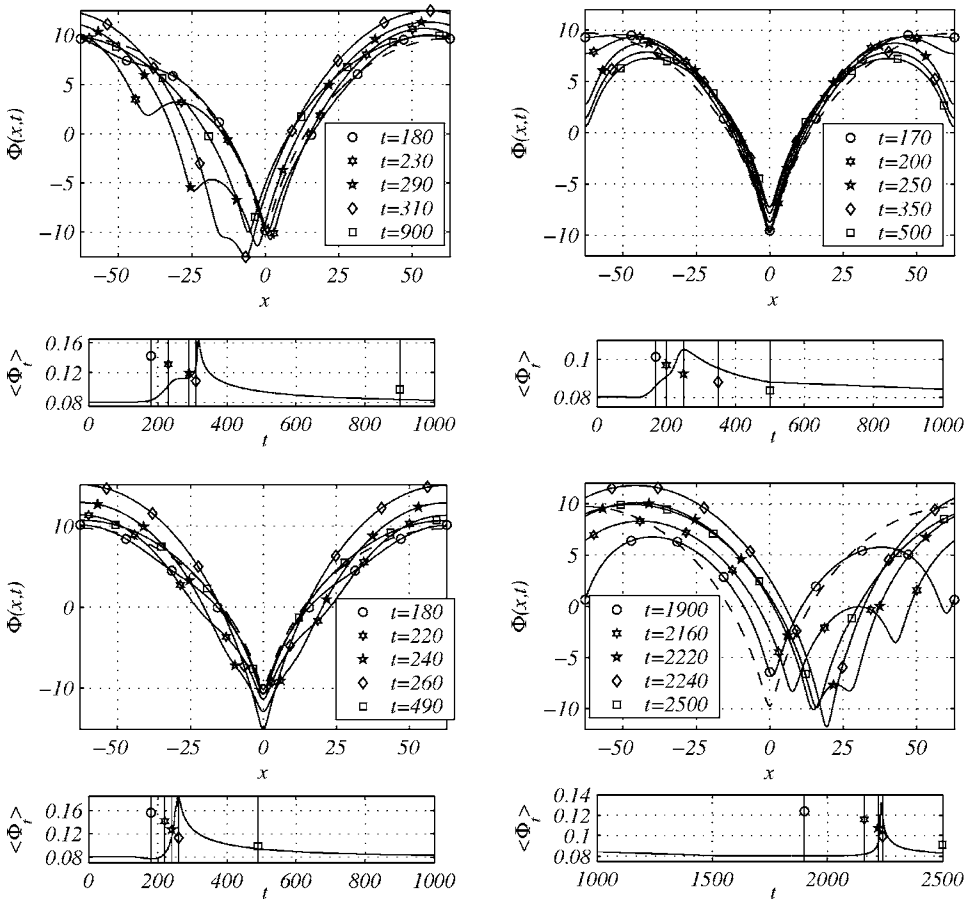

FIG. 4. Solutions to Eq. (1) for $\Phi(x,0)=\Phi_L+\varepsilon\psi_\alpha(x,t^*)$ and $L=40\pi$. The dashed line corresponds to Eq. (2) with $\langle\Phi_t\rangle=V_L=0.08$. Here $\alpha=1$ in the top left and $\varepsilon=-10^{-3}$ in the bottom right; $\alpha=2$ and $\varepsilon=10^{-3}$ in all other places.

illustrated in Fig. 4. All the profiles were displaced vertically in order to compensate for steady propagation of flames in such a way that their spatial averages are equal to zero. Matching graphs of the spatially averaged flame propagation speed

$$\langle\Phi_t\rangle=\frac{1}{L}\int_{-L/2}^{L/2}\partial_t\Phi(x,t)dx \tag{8}$$

are shown as well. The initial conditions were $\Phi(x,0)=\Phi_L(x,0)+\varepsilon\psi_\alpha(x,t^*)$, where $\varepsilon=\pm10^{-3}$, $\alpha=1,2$, and $t^*=10^3$. The computational method used in this work was presented in [8].

The asymmetric singular mode $\psi_1(x,t^*)$ results in the appearance of a small cusp to the left or to the right from the trough of $\Phi_L(x,0)$ depending on the sign of ε. After the cusp merges with the trough, the flame profile converges slowly to $\Phi_L(x+\Delta x,t)$, where $\mathrm{sgn}(\varepsilon)\Delta x>0$. For a positive $\varepsilon=10^{-3}$ the effect is illustrated in Fig. 4 (top left). Graphs of $\Phi(x,t)$ for $\varepsilon=-10^{-3}$ are exact mirror reflections of those depicted in Fig. 4 (top left), and graphs of $\langle\Phi_t\rangle$ are exactly the same.

The symmetric singular mode $\psi_2(x,t^*)$ produces two symmetric dents moving towards the trough on both sides of the profile if $\varepsilon<0$; see Fig. 4 (bottom left). By $t\approx500$ the flame profile returns very closely to $\Phi_L(x,t)$. For $\varepsilon>0$ two small cusps move towards the boundaries of the computational domain, creating a quasisteady structure shown in Fig. 4 (top right) for $t=270$. This structure survives until $t\approx1800$, but eventually bifurcates [see Fig. 4 (bottom right)], and the solution converges to $\Phi_L(x+\Delta x,t)$, $\Delta x<0$. It looks like the bifurcation in question is associated with the lack of asymptotic stability of the intermediate quasisteady structure. As such, it was triggered by a random perturbation and could equally result in the displacement of the limiting flame front profile into the opposite direction $\Delta x>0$.

The behavior of perturbations $\psi_\alpha(x,t^*)$, $\alpha=1,2$, of amplitude $\varepsilon=10^{-6}$ was not as impressive, but they managed to produce a visible effect on the flame front profile. The same can be said about $\psi_\alpha(x,t^*)$, $\alpha=3,4$, of amplitude $\varepsilon=10^{-3}$. Perturbations corresponding to $\psi_\alpha(x,t^*)$ of higher orders did not grow significantly and did not cause any noticeable changes to Φ_L for ε up to 10^{-2}.

Thus, the singular modes $\psi_\alpha(x,t^*)$, $\alpha=1,2$, should be responsible for the interaction of the flame front $\Phi_L(x,t)$ with all the perturbations of small enough amplitude. The time scale of these interactions is about 300 for $L=40\pi$ and is of order $O(L)$ in general. More singular modes $\psi_\alpha(x,t^*)$ of higher orders $\alpha>2$ are becoming important as the amplitude of the perturbations grows. The time scale of evolution of $\phi(x,t)$ for $\phi(x,0)=\psi_\alpha(x,t^*)$ lessens as α grows, necessitating taking into account the dependence of $\psi_\alpha(x,t^*)$ on t^* and creating further problems in the efficient description of the subspace of important perturbations. Therefore, there is a critical perturbation amplitude beyond which the representation of $f(x,t)$ in terms of the singular modes $\psi_\alpha(x,t^*)$ is not as beneficial as for smaller amplitudes.

In other words, in relation to noise the Sivashinsky equation (1) works as a very sensitive nonlinear filter, responding to very exceptional perturbations only. Those allowed perturbations are hugely amplified by a linear transient mechanism and eventually develop into cusplike structures during the nonlinear stage of their evolution. These cusplike structures can speed up the flame front significantly. From physical point of view, the cusplike structures are formed by pairs of vortexes located on both sides of the cusp just behind the flame front. Their size is of order of the neutral wavelength $4\pi/\gamma$.

Calculations of this section were carried out for a variety of flame sizes $20\pi \leqslant L \leqslant 80\pi$. Qualitatively, the results are the same as those illustrated here for $L=40\pi$. There are always two types of the mostly growing perturbations, which can be amplified up to about $e^{O(L)}$ times; cf. [7,11]. Perturbations from the orthogonal supplement are amplified at least a few orders of magnitude less. Singular vectors $\psi_\alpha(x,t^*)$ scale with L, and the behavior of solutions (2) perturbed with $\varepsilon\psi_\alpha(x,t^*)$, $\alpha=1,2$, is the same as illustrated in Fig. 4. The same quantitative effects can be observed for larger flames using smaller values of ε in proportion with $e^{-O(L)}$. Characteristic time scales vary in proportion with L. For $L \gtrsim 70\pi$ round-off errors become apparent and appropriately extended machine arithmetic with at least $O(L/\pi)$ binary digits is required to reduce them to an acceptable level; see also [11].

The numerical algorithm used in this work to solve Eq. (1) is essentially the same spectral method, which was routinely employed by many researchers earlier; see, e.g., [13]. Briefly, the computational formulas are obtained by linearly extrapolating the nonlinear term of Eq. (1) in the Fourier space from the subsequent time instances t_{n-1} and t_n to the interval $[t_{n-1},t_{n+1}]$ and then integrating the resulting linear decoupled system of ordinary differential equations (ODE's) over this interval. For smooth enough solutions such an approach provides a second-order approximation in time. The most important thing is that the approximation error is nearly orthogonal to the subspace of the mostly growing perturbations. Thus, during the linear stage, when most of the amplification takes place, the perturbation caused by the approximation residual and our special perturbations $\varepsilon\psi_\alpha(x,t^*)$, $\alpha=1,2$, are effectively decoupled and do not interfere with each other. Further details of the impact of the high sensitivity of the Sivashinsky equation to certain perturbations on its numerical treatment are discussed in [8].

The numerical simulations of the Sivashinsky equation presented in this work were carried out using the time step $\Delta t=0.01$ and the number of modes $K=256$ for $L\leqslant 40\pi$ and $K=512$ for $40\pi < L \leqslant 80\pi$. The results were checked via calculations with smaller time steps and larger number of modes and were found to stabilize for $\Delta t \lesssim 0.05$ and $K \gtrsim 2L/\pi$. The latter inequality can also be interpreted as a necessity to have at least a dozen of harmonics with wavelengths less than the neutral one $\lambda=4\pi/\gamma$.

III. LINEAR ANALYSIS IN THE CREST OF A FLAME CELL

The crest is the most critical part of the flame cell from the point of view of its stability. In particular, the graphs in Fig. 2 demonstrate that most intensive variations of ψ_α's occur near the crest, which is located at $x=\pm 20\pi$ in the system of coordinates used in those graphs. Therefore, in this section we will complement computational studies of the set of functions $e^{tA_L}\phi(x,0)$ versus $\phi(x,0)$ and t, carried out in the previous section on $x\in[-L/2,L/2]$, with analytical estimations in a vicinity of the crest, $x\approx \pm L/2$.

The L-periodic steady coalescent N_L-pole solution (2) can be represented in a vicinity of the crest as $\Phi_L(x,t) \approx \Phi_L(0,t)-x^2/(2R)+O(x^4)$. Here, R is the radius of curvature of the flame front profile in the crest. For large enough L, it can be approximated as $R\approx c_1L+c_2$, where c_1 and c_2 are some constants. Note that here the origin $x=0$ was chosen exactly in the crest of $\Phi_L(x,t)$. Thus, $\partial_x\Phi_L \approx -x/R+O(x^3)$ in a vicinity of $x=0$ and Eqs. (3) are transformed into

$$\partial_t\phi + R^{-1}x\partial_x\phi = \partial_{xx}\phi + (\gamma/2)\partial_x\mathcal{H}[\phi] + f(x,t). \tag{9}$$

In general, Eq. (9) is only valid in a small vicinity of $x=0$. However, assuming that perturbations appear only in the crest, one may consider Eq. (9) on $-\infty < x < \infty$ over intervals of time up to $O(R)$; see [9].

Equation (9) can be solved exactly. Applying the Fourier transformation we obtain

$$\partial_t\mathcal{F}[\phi] - R^{-1}\xi\partial_\xi\mathcal{F}[\phi] = -(4\pi^2\xi^2 - \pi\gamma|\xi| - R^{-1})\mathcal{F}[\phi] + \mathcal{F}[f](\xi,t), \tag{10}$$

which is a linear nonhomogeneous hyperbolic equation of the first order. Using the standard method of characteristics its exact solution can be written as

$$\mathcal{F}[\phi](\xi,t) = \mathcal{G}(\xi,t)\mathcal{F}[\phi^{(0)}](|\xi|e^{t/R}) + \int_0^t \mathcal{G}(\xi,t-\tau)\mathcal{F}[f] \times[|\xi|e^{(t-\tau)/R},\tau]d\tau, \tag{11}$$

where

$$\mathcal{G}(\xi,t) = e^{t/R-2\pi^2R(e^{2t/R}-1)\xi^2+\pi\gamma R(e^{t/R}-1)|\xi|} \tag{12}$$

and $\mathcal{F}[f](\xi,t)=\int_{-\infty}^{\infty}f(x,t)e^{-i2\pi x\xi}dx$ denotes the Fourier transformation of $f(x,t)$.

If the initial condition is a single harmonics $\phi^{(0)}(x) = \cos(2\pi\xi_0 x+\varphi)$ and $f(x,t)\equiv 0$, then

$$\phi(x,t) = e^{-2\pi^2R(1-e^{-2t/R})\xi_0^2+\pi\gamma R(1-e^{-t/R})\xi_0}\cos(2\pi\xi_0 x e^{-t/R}+\varphi). \tag{13}$$

The infinite-time limit of Eq. (13) is equal to $e^{-2\pi^2R\xi_0^2+\pi\gamma R\xi_0}\cos\varphi$ and is reached effectively on the time scale of order $O(R)$. This time limit attains its maximum $e^{\gamma^2R/8}\cos\varphi$ for $\xi_0=\xi^*=\gamma/(4\pi)$, matching the asymptotic estimation of [9]. The argument of the cosine in Eq. (13) depends on time, which means that even if the initial condition $\phi^{(0)}(x)$ is a linear combination of mutually orthogonal cosine harmonics, then the solution $\phi(x,t)$ will remain a linear combination of cosine harmonics for $t>0$, but those harmonics will no longer be mutually orthogonal. This explains why the most amplified perturbations are formed by linear combinations of a few initially orthogonal harmonics and approximate $\psi_\alpha(x,t^*)$, $\alpha=1,2$, asymptotically for $L\to\infty$. Note that the wave number of the largest Fourier component k^* of both $\psi_1(x,t^*)$ and $\psi_2(x,t^*)$ for $t^*>300$ is equal to $\xi^*=k^*/L=\gamma/(4\pi)$ as well; see Fig. 3.

The behavior of Eq. (13) is in a sharp contrast with the evolution of the single-harmonics perturbations of the plane flame front,

$$\phi(x,t)=e^{(-4\pi^2\xi_0^2+\pi\gamma\xi_0)t}\cos(2\pi\xi_0 x+\varphi), \tag{14}$$

which grow infinitely if $\xi_0<\gamma/(4\pi)$ or decay otherwise. They are governed by the equation associated with a self-adjoint differential operator, which is obtained from Eq. (9) upon removal of the term $R^{-1}x\partial_x\phi$. Solution (14) does not result from Eq. (13) for $R\to\infty$, but is only equivalent to it when $t/R\ll 1$. The difference between Eqs. (13) and (14) is an explicit illustration of the nonnormality of Eq. (9) introduced by the non-self-adjoint term $R^{-1}x\partial_x\phi$. Flattening of the crests of cellular flames and bettering of their local resemblance with the plane front as R grows was noticed long time ago, prompting a hypothesis of a secondary Darrieus-Landau instability. Model (9) indicates that the hypothesis is unlikely to be correct. Although because of the flattening of the crests of the flame front profile perturbations of the front can be transiently amplified at a rate rapidly increasing with R, this transient amplification is entirely different from the infinite growth of perturbations in the Darrieus-Landau instability of plane flames. Moreover, the dynamics of perturbations in the case of cellular flames does not converge to that of the plane ones continuously in the limit $R\to\infty$.

Solution (11) and (12) for $\phi(x,0)=e^{-px^2}$, $p>0$, can be represented in a closed form as well. Routine integration yields

$$\phi(x,t)=\frac{\pi}{\sqrt{pa}}e^{t/R+(b^2-4\pi^2x^2)/4a}\left\{\cos\frac{\pi bx}{a}+\mathrm{Re}\left[e^{i\pi bx/a}\,\mathrm{erf}\left(\frac{b+i2\pi x}{2\sqrt{a}}\right)\right]\right\}, \tag{15}$$

where

$$a=a(t)=2\pi^2R(e^{2t/R}-1)+\pi^2e^{2t/R}/p,$$

$$b=b(t)=\pi\gamma R(e^{t/R}-1). \tag{16}$$

Graphical illustrations of Eqs. (13), (15), and (16) can be found in [14].

The steady coalescent pole solutions to the Sivashinsky equation correspond to the flame fronts propagating steadily with the velocity exceeding $u_b=1$ by $V_L=2\pi NL^{-1}(\gamma-4\pi NL^{-1})$; see, e.g., [13]. Addition of the perturbation $\phi(x,t)$ results in a change in the velocity of propagation by the value of the space average of $\partial_t\phi$, which we denote $\langle\phi_t\rangle$. The correction provided by the $\phi(x,t)$ is only valid in a small vicinity of the crest of $\Phi_L(x,t)$. In sequel, the correction of the speed $\langle\phi_t\rangle$ is only valid for a small region $-\varepsilon\leqslant x\leqslant\varepsilon$ of the flame front in a vicinity of the crest of $\Phi_L(x,t)$. Hence, for our simplified linear model we define the increase of the flame propagation speed as follows:

$$\langle\phi_t\rangle=\frac{1}{2\varepsilon}\int_{-\varepsilon}^{\varepsilon}\partial_t\phi dx\approx\ \partial_t\phi|_{x=0}. \tag{17}$$

For the single-harmonics solution (13) the expression for $\langle\phi_t\rangle$ is obvious and demonstrates the high sensitivity of $\langle\phi_t\rangle$ to the wavelength of the perturbation. The phase, or location of the perturbation, is important as well.

IV. EFFECT OF NOISE

According to the results of Sec. II, the forcing in the Sivashinsky equation can be decomposed into the most amplifiable nonmodal component and orthogonal complement. The latter can be neglected reducing spatiotemporal stochastic noise to the appearance of a sequence of the most growing perturbations $\psi_{\alpha_m}(x,t^*)$, $1\leqslant\alpha_m\leqslant\alpha^*=\alpha^*(f_0)$, at a set of time instances t_m, $m=0,1,2,\ldots$:

$$f(x,t)\approx f_0\sum_{m=0}^{\infty}\psi_{\alpha_m}(x,t^*)\,\delta(t-t_m),$$

$$1\leqslant\alpha_m\leqslant\alpha^*=\alpha^*(f_0). \tag{18}$$

Thus, the amplitude of noise f_0, alongside the averages and the standard deviations of $t_{m+1}-t_m$ and α_m, $m=0,1,2,\ldots$, are the only essential parameters of such a representation of noise.

The impulselike noise (18) is used here for the sake of simplicity. Some arguments towards its validity were suggested in [2]. More sophisticated and physically realistic models of temporal noise characteristics can be used with Eq. (1) as well.

If $f_0\ll\sigma_1^{-1}(t^*)$, then noise is not able to affect the flame at all and can be completely neglected. This case can be referred to as the noiseless regime. On the other hand, if f_0 is comparable with the amplitude a of the background solution $\Phi_L(x,t)$, then almost all components of noise will be able to disturb the flame and the $f(x,t)$ in Eq. (1) should be treated as a genuine spatiotemporal stochastic function. This is the regime of the saturated noise.

Eventually, there is an important transitional regime when the noise amplitude f_0 is at least of order of $\sigma_1^{-1}(t^*)$, but still much smaller than a. In this case only the disturbances with a significant component in the subspace spanned by the linear combinations of $\psi_\alpha(x,t^*)$, $1\leqslant\alpha\leqslant\alpha^*$, have a potential to affect the solution. All other disturbances can be neglected, and the force $f(x,t)$ in the Sivashinsky equation (1) can be approximated by Eqs. (18) with a finite value of α^*. We would like to stress that though such representation of noise is correct for noise of any amplitude, apparently it is only efficient if $f_0<\sigma_{\alpha^*}^{-1}(t^*)\ll a$, where α^* is small enough.

A. Noise in the linear model

A random pointwise set of perturbations uniformly distributed in time and in the Fourier space is a suitable model for both the computational round-off errors and a variety of

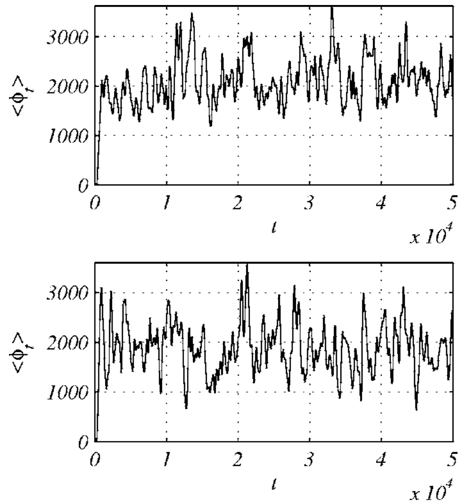

FIG. 5. The effect of noise (19) on $\langle \phi_t \rangle$ for $L=40\pi$ and $a_m \in [0,1]$; $F=1$, $\xi_m \in [0,1]$ in the top and $F=1/33$, $\xi_m=\gamma/(4\pi)$ in the bottom.

perturbations of physical origins. We are adopting such a model in our analysis in the form

$$f(x,t) = \sum_{m=1}^{M(t)} a_m \cos(2\pi\xi_m x + \varphi_m)\,\delta(t-t_m), \qquad (19)$$

where a_m, t_m, ξ_m, and φ_m are noncorrelated random sequences. It is assumed that $t_1 \leqslant t_2 \leqslant \cdots \leqslant t_m \leqslant \cdots \leqslant t_{M(t)} \leqslant t$, $0 \leqslant \varphi_m \leqslant 2\pi$, and $\xi_m \geqslant 0$, $m=1,2,\ldots,M(t)$. Availability of the exact solution (15) makes it also possible to study an alternative noise model based on elementary perturbations $a_m e^{-p_m(x-x_m)^2}$, which are local in physical space.

Using Eqs. (11) and (12) for the zero initial condition, the exact solution to Eqs. (9) and (19) can be written as

$$\phi(x,t) = \sum_{m=1}^{M(t)} a_m \cos[2\pi\xi_m e^{-(t-t_m)/R}x + \varphi_m] \times e^{-2\pi^2 R[1-e^{-2(t-t_m)/R}]\xi_m^2 + \pi\gamma R[1-e^{-(t-t_m)/R}]\xi_m}. \qquad (20)$$

The expression for $\langle \phi_t \rangle$ is obvious [see Eq. (17)] and is illustrated in Fig. 5. Here we generated random sequences of the time instances t_m with a given frequency $F=M(T)/T$ on a time interval $t \in [0,T]$. Values of the wave number ξ_m and of the amplitude a_m were also randomly generated and uniformly distributed within certain ranges. According to the formula for $\langle \phi_t \rangle$, the effect of the phase shift φ_m just duplicates the a_m. Therefore, its value was fixed as $\varphi_m \equiv 0$.

If values of a_m are uniformly distributed in $[-1,1]$, then the time average of $\langle \phi_t \rangle$ is obviously zero, because of the linearity of the problem. In the Sivashinsky equation this effect is compensated by the nonlinearity. The cusps generated by the perturbations of opposite signs move into opposite directions along the flame surface (see Sec. II), though they both contribute to the speed positively. This effect of the nonlinearity can be mimicked by restricting the range of possible values of the amplitudes—e.g., $a_m \in [0,1]$—as this can be seen in Fig. 5.

Figure 5 (bottom) shows that the increase of $\langle \phi_t \rangle$ seen in Fig. 5 (top) can be matched by using only the largest growing perturbations with much smaller frequency, which is quite expected in virtue of the linearity of the problem. The amplitude of fluctuations in Fig. 5 (top) is noticeably less than in Fig. 5 (bottom). This is attributed to the smoothing effect of the less growing perturbations.

Because of the linearity of the problem in question, the effect of $F=M(T)/T$ and L on $\langle \phi_t \rangle$ is straightforward. In particular, the value of $\langle \phi_t \rangle$ rises up to about 4×10^8 for $L=80\pi$ and other parameters the same as in Fig. 5 (top). It should be noticed, however, that because of the limitation $a_m \geqslant 0$, the quantity $\langle \phi_t \rangle$ do no longer represents the increase of propagation speed of the flame, but is just a measure of the rate of transient amplification of perturbations; see also [7,8].

Direct studies of the effect of noise in the Sivashinsky equation necessitate use of numerical simulations. However, because of the intrinsic discontinuity of noise, such direct numerical simulation (DNS) are hampered with very low accuracy of approximations, questioning the validity of numerical solutions. In this work we used explicit solutions (20) in order to validate DNS of Eq. (9) and, in sequel, of Eq. (1). The DNS of Eqs. (9) and (19) was carried out using a spectral method briefly outlined in the end of Sec. II. The delta function was approximated as

$$\delta(t-t_m) \approx \frac{1}{\sqrt{\pi\tau}} e^{-(t-t_m)^2/\tau}, \quad \tau \ll 1/F. \qquad (21)$$

The calculations have shown that discrepancies between Eq. (20) and its numerical counterparts obtained with the same sets of t_m, a_m, and ξ_m might be noticeable in a neighborhood of the time instances $t \approx t_m$, although the averaged characteristics like $\langle \phi_t \rangle$ were quite accurate. So this linear model validates the DNS of the forced Sivashinsky equation at least in relation to the averaged flame propagation speed.

B. Sivashinsky equation

We carried out a series of computations of Eqs. (1) and (18) with $\Phi_L(x,t)$ as initial condition and with a variety of parameters of the noise term. Up to 12 basis functions $\psi_\alpha(x,10^3)$, where α was uniformly distributed in the interval $1 \leqslant \alpha \leqslant \alpha^* \leqslant 12$, were used. The sign of f_0 in Eqs. (18) was either plus or minus for every m with the equal probability $1/2$ and the delta function $\delta(t-t_m)$ was approximated according to Eq. (21).

The effect of the amplitude of noise on the flame speed is illustrated in Fig. 6. Use of only two basis functions $\psi_\alpha(x,10^3)$, $\alpha=1,2$, gives almost the same result. Similar to the linear model (9) the only noticeable difference was in slightly larger fluctuations of $\langle \Phi_t \rangle$.

It was mentioned in the previous section that the wave number of the largest Fourier component of $\psi_\alpha(x,10^3)$,

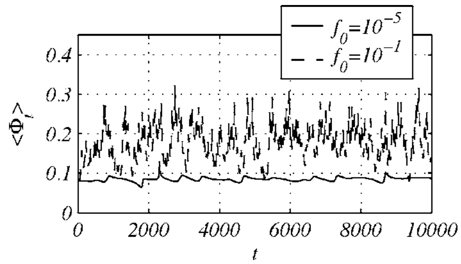

FIG. 6. The effect of the amplitude of noise (18) on $\langle\Phi_t\rangle$ for $L=40\pi$. Here $F=1/15$ and $\alpha^*=12$.

$\alpha=1,2$, is exactly the same as the wave number $\xi_0=\gamma/(4\pi)$ of the largest growing single harmonics solution to Eq. (9). We tried to exploit this observation and simplified Eqs. (18) even further, replacing $\psi_{\alpha(m)}(x,t^*)$ by $\cos(\gamma x/4)$, which corresponds to ξ_0—i.e.,

$$f(x,t) \approx f_0 \cos\frac{\gamma x}{4}\sum_{m=0}^{\infty}\delta(t-t_m). \qquad (22)$$

This kind of forcing is able to speed up the flame, but the difference between the computational results obtained with Eqs. (18) and (22) is noticeable. It does not disappear even if eight nearest sidebands are added to Eq. (22).

The time averages of $\langle\Phi_t\rangle$, denoted here as

$$\langle\langle\Phi_t\rangle\rangle = \frac{1}{t_{end}-t_0}\int_{t_0}^{t_{end}}\langle\Phi_t\rangle dt, \qquad (23)$$

are depicted in Fig. 7 versus F and f_0. Discrepancies in $\langle\langle\Phi_t\rangle\rangle$ for different α^* did not exceed the variations caused by the different randomly chosen sequences of t_m, although the effect of using Eq. (22) instead of Eqs. (18) is appreciable.

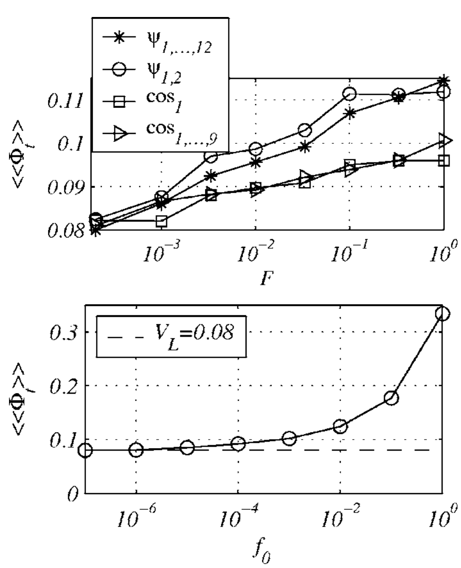

FIG. 7. The effect of the composition (top) and amplitude (bottom) of noise on the spatiotemporally averaged flame propagation speed $\langle\langle\Phi_t\rangle\rangle$. Here $L=40\pi$ and the temporal averaging was over the interval $t\in[200,10^4]$, $f_0=10^{-3}$ (top), $F=1/15$, $\alpha^*=12$ (bottom).

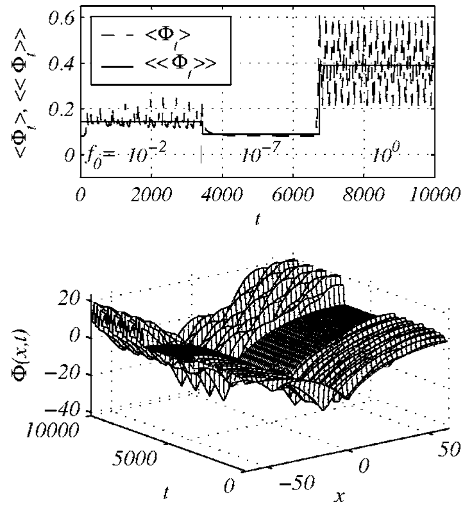

FIG. 8. An example of controlling the flame speed with the amplitude of the perturbations f_0. Here $F=1/15$, $\alpha^*=12$, and $L=40\pi$.

The correlation between the flame propagation speed and the noise amplitude is obvious. Note that the f_0 in the rightmost point in the graph is still about 20 times less than the amplitude of the variation of the background solution $\Phi_L(x,t)$.

In accordance with the idea developed in this paper, the value of $\langle\langle\Phi_t\rangle\rangle$ is determined by the product $\sigma_1 f_0$. It was shown in [7] that $\sigma_1 \propto e^{O(L)}$, resulting in $\langle\langle\Phi_t\rangle\rangle=\langle\langle\Phi_t\rangle\rangle(e^{O(L)}f_0)$. Thus, the data shown in Fig. 7 are at least in a qualitative agreement with the dependence of $\langle\langle\Phi_t\rangle\rangle$ on L, which was obtained in [7] for a fixed noise amplitude $f_0\approx 10^{-16}$ associated with the computational round-off errors.

Eventually, in Fig. 8 we present the results of an attempt to control the flame propagation speed using our special perturbations $\psi_\alpha(x,t^*)$ of properly selected amplitudes. Graphs of $\langle\Phi_t\rangle$ and $\langle\langle\Phi_t\rangle\rangle$ are shown in the top and numerical solution $\Phi(x,t)$ corresponding to this controlling experiment is illustrated in the bottom. The fluctuations of the obtained flame propagation speed are large indeed, but at least, they appear in quite a regular pattern.

In this paper noise or forcing in Eq. (1) represents the turbulence of the upstream velocity field, which is difficult to manage in practice. The controlling function is more effectively achieved by acoustic signals; see, e.g., [15]. Acoustics was neglected in the evaluation of the Sivashinsky equation, and there is no easy and straightforward way to incorporate it back into the model. However, because of a strong coupling between the velocity and pressure fields, effects of acoustic signals similar to those presented here can be expected as well.

V. CONCLUSIONS

Based on our analysis of the steadily propagating cellular flames governed by the Sivashinsky equation we may conclude that there are perturbations of very small amplitude, which can essentially affect the flame front dynamics. The subspace formed by these special perturbations is of a very small dimension, and its basis can be used for an efficient representation of the upstream velocity turbulence. These are the very perturbations which cause the increase of the flame propagation speed in numerical experiments. Hence, theoretically, they can be used to model certain regimes of flame-turbulence interaction and to control the flame propagation speed on purpose.

ACKNOWLEDGMENT

The research presented in this paper was supported by EPSRC Grant No. GR/R66692.

[1] G. Sivashinsky, Acta Astron. **4**, 1177 (1977).
[2] G. Joulin, Combust. Sci. Technol. **60**, 1 (1988).
[3] G. Joulin and P. Cambray, Combust. Sci. Technol. **81**, 243 (1992).
[4] P. Cambray and G. Joulin, *Proceedings of the Twenty-Fourth Symposium (International) on Combustion*, Sydney, Australia, 1992 (Combustion Institute, Pittsburgh, PA, 1993), pp. 61–67.
[5] O. Thual, U. Frisch, and M. Hénon, J. Phys. (Paris) **46**, 1485 (1985).
[6] D. Vaynblat and M. Matalon, SIAM J. Appl. Math. **60**, 679 (2000).
[7] V. Karlin, Proc. Combust. Inst. **29**, 1537 (2002).
[8] V. Karlin, V. Maz'ya, and G. Schmidt, J. Comput. Phys. **188**, 209 (2003).
[9] G. Joulin, J. Phys. (Paris) **50**, 1069 (1989).
[10] I. Gohberg and M. Krein, *Introduction to the Theory of Linear Nonselfadjoint Operators* (AMS, Providence, RI, 1969).
[11] V. Karlin, Math. Methods Appl. Sci. **14**, 1191 (2004).
[12] G. Golub and C. van Loan, *Matrix Computations* (The Johns Hopkins University Press, Baltimore, 1989).
[13] M. Rahibe, N. Aubry, and G. Sivashinsky, Combust. Theory Modell. **2**, 19 (1998).
[14] V. Karlin, e-print physics/0502036.
[15] C. Clanet and G. Searby, Phys. Rev. Lett. **80**, 3867 (1998).